First paleomagnetic and $^{40}Ar/^{39}Ar$ study of Paleoproterozoic rocks from the French Guyana (Camopi and Oyapok rivers), northeastern Guyana Shield

S. Nomade [a], Y. Chen[a], G. Féraud[b], A. Pouclet[a] and H. Théveniaut[c]

[a] ISTO, Université d'Orléans, rue de St Amand, 45067 Orléans Cedex 2, France
[b] CNRS, UMR 6525 Géosciences Azur, Université de Nice–Sophia Antipolis, 06108 Nice Cedex 2, France
[c] BRGM, SGN, 3 avenue Claude Guillemin, B.P. 6009, 45069 Orléans Cedex 2, France

Abstract

In order to understand the Paleoproterozoic geographic evolution of the Guyana Shield, paleomagnetic and $^{40}Ar/^{39}Ar$ investigations were carried out on granitoids and volcano-sedimentary rocks from the Oyapok and Camopi rivers (French Guyana–Brazil frontier). Scanning electronic microscope, thermomagnetic and isothermomagnetic experiments show that magnetite is the main magnetic remanent carrier in most of the samples. The metavolcano-sedimentary rocks (Paramaca) show a weak magnetization and scattered magnetic directions. Therefore, no reliable magnetic component could be isolated from these samples. Samples taken from tonalite and meta-ultrabasite rocks yield a characteristic magnetic direction, carried by subautomorphous magnetite, that is well defined and distinct from that of the present Earth field and that of nearby Jurassic dikes. A virtual geomagnetic pole (VGP) deduced from this probable primary remanence was calculated, namely pole OYA, λ=28.0°S, φ=346.0°E, N=5, k=31.9 and A_{95}=13.8°. Four $^{40}Ar/^{39}Ar$ ages, ranging from 2052 to 1973 Ma, were obtained from amphiboles and biotites of tonalite rocks, showing a relatively slow cooling rate of ca 4.8+2.6/−2.1°C Ma^{-1}. The linear extrapolation of this cooling rate to the magnetite unblocking temperature (540 to 580°C) yields a magnetization age of 2036±14 Ma for pole OYA. Pole OYA differs significantly from available paleomagnetic results from Venezuela of the West Guyana Shield dated at 2000±10 Ma. This difference may indicate an important latitudinal movement of the Guyana Shield between 2036 and 2000 Ma with a velocity of 9±7 cm/year.

Author Keywords: Guyana Shield; paleomagnetism; $^{40}Ar/^{39}Ar$ dating; Paleoproterozoic

1. Introduction

Paleomagnetism, for decades, has provided important constraints on the geodynamic history of the Earth. Most of the available data (77%) were obtained on Phanerozoic rocks (Global Paleomagnetic Database version 3.3; GPMDB, 1998). Only 7% concern the Paleoproterozoic period, which occupies 20% of Earth history. Recent paleomagnetic data concerning the Fennoscandian Shield (Torsvik and Fedotova; Mertanen et al., 1999) and North American Shield (Buchan et al., 1996) yielded new paleogeographic constraints between these two zones during this period. Most of these investigations were conducted on intrusive rocks and were associated with U/Pb dating (Buchan; Fedotova and Mertanen). The magnetic remanence age in quickly cooled volcanic rocks and dikes is close to the U/Pb age, but in slowly cooled Precambrian terrains the age of acquisition of thermal remanent magnetization (TRM) cannot always be directly defined by one isotopic method. The slow cooling rate is

generally attributed to gradual uplift and erosion. In order to estimate the magnetic remanence age more precisely, the combined study of the paleomagnetism with $^{40}Ar/^{39}Ar$ thermochronology is important and sometimes critical (Berger; Costanzo and Briden).

In the framework of a multidisciplinary BRGM (Bureau de Recherche Géologique et Minière) geological mapping project of the French Guyana Territory in collaboration with Orleans Institut of Geosciences (ISTO), UMR-CNRS 6527 and the CPRM (Brazilian geological survey), we carried out two field trips in 1997 and 1998. This study presents new time-calibrated paleomagnetic data from the northeastern part of the Guyana Shield. The $^{40}Ar/^{39}Ar$ data allow one to evaluate the cooling rate for the central Oyapok/Camopi zone at about 2 Ga for the first time. Paleogeographic and tectonic implications of paleomagnetic results are then discussed with previous studies from the northwest part of the Guyana Shield (Fig. 1, Onstott; Onstott and Onstott).

2. Geological setting and sampling

2.1. Regional and local geology

The Guyana Shield is composed of a narrow Archean belt (Imataca Complex in Venezuela) and of granite–greenstone belts (2.2 to 2.0 Ga), formed during the Transamazonian tectonothermal event (Fig. 1; Montgomery and Teixieira). Two major strike-slip fault zones cross the Guyana Shield: (1) the Guri fault zone (GFZ) separates the Archean belt from the Paleoproterozoic series; (2) the Pisco Jurua fault (PJF) is located on the western border of the Central Guyana Granulite Belt (CGGB) and extends from western Suriname to Roraima State, Brazil (Fig. 1), thus dividing the shield into two parts (Fig. 1). The PJF is interpreted as a mobile belt reflected by the charnockitization of older rocks (Dahlberg and Gibbs and Baron, 1993). French Guyana is situated in the northeastern part of the Guyana Shield (Fig. 1). The Paleoproterozoic lithological succession is well known in the Oyapok–Camopi rivers; the basement is composed of the Paramaca greenstone belt sequence (Fig. 2). It is constituted by volcanic rocks with tholeiitic and calc-alkaline compositions (Mil and Egal et al., 1995) dated at 2110±90 Ma (Sm/Nd age, Gruau et al., 1985). These volcanic rocks are covered by sedimentary deposits of Armina (Fig. 2, Ledru et al., 1991). The volcano-sedimentary rocks are metamorphosed and deformed by the Guyana and Caribbean granite intrusions (Fig. 2, Choubert, 1974), which are dated at 2130 to 2080 Ma (Pb/Pb ages, Vanderhaeghe et al., 1998). All these rocks are crosscut by Mesozoic dikes (Fig. 2) associated with the Central Atlantic Ocean prerifting stages (Deckart et al., 1997). This latest volcanic event constitutes the only major thermal event since the Early Paleoproterozoic in French Guyana.

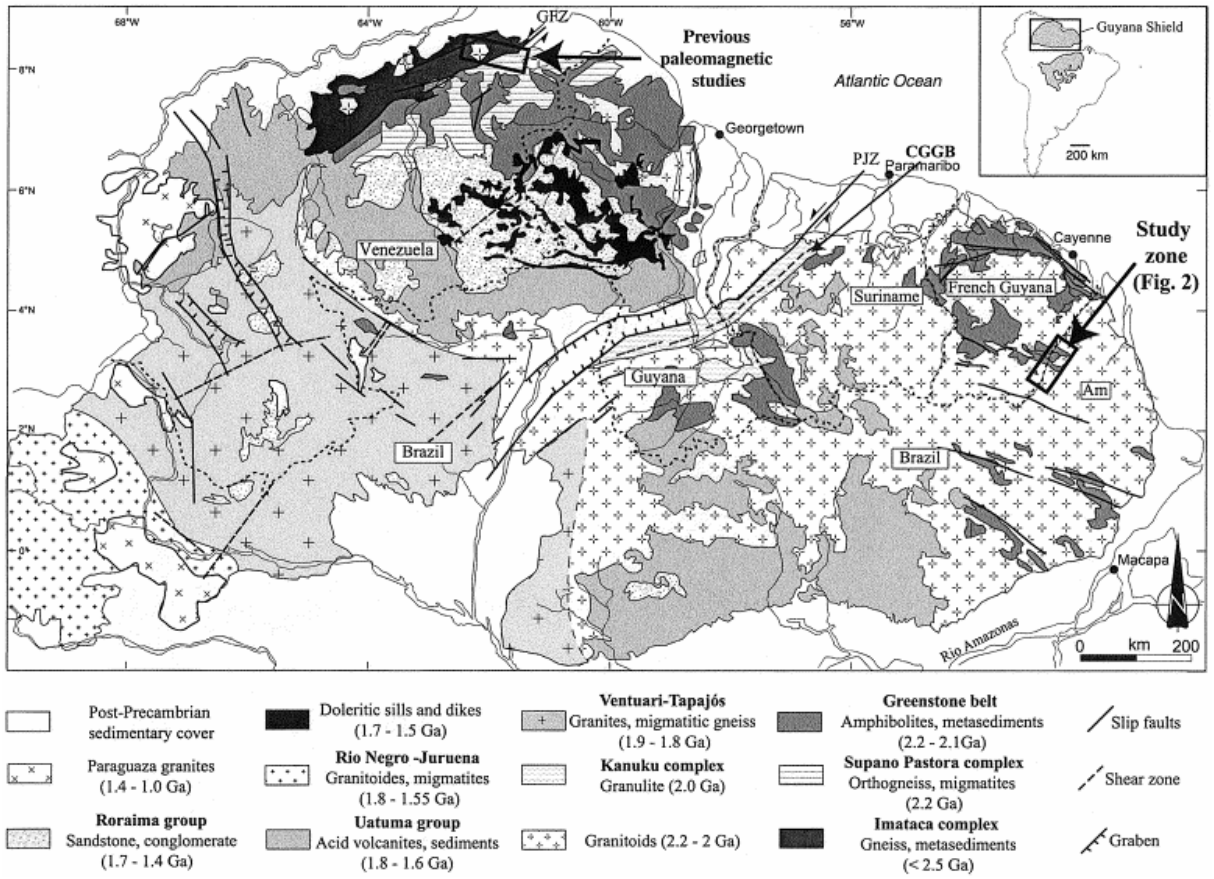

Fig. 1. Geological map of Guyana Shield (modified after Gibbs and Baron (1993)). CGGB: Central Guyana Granulitic belt. GFZ: Guri fault zone; PJZ: Pisco Jurua fault zone. Our study zone and previous paleomagnetic sampling are indicated.

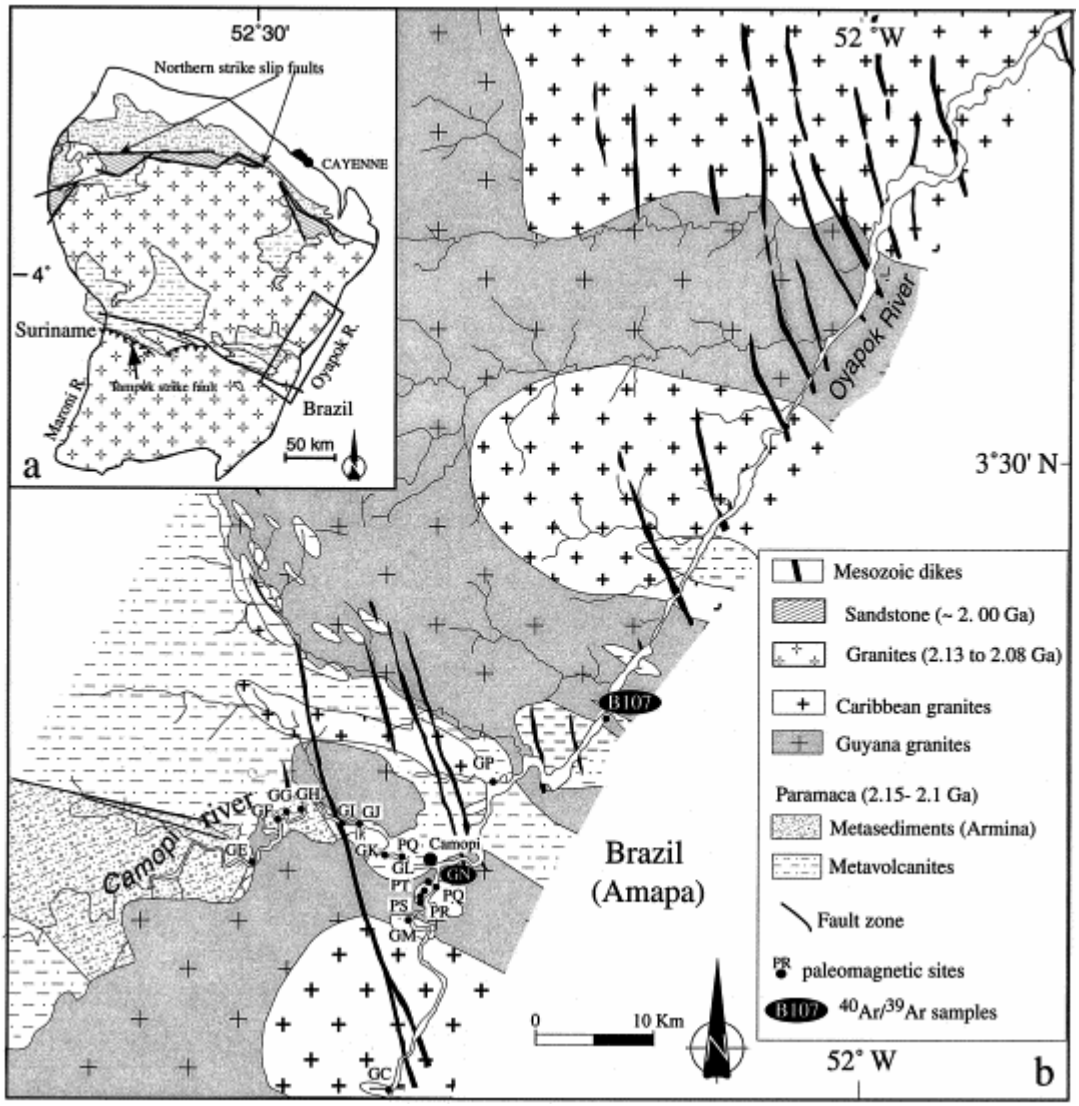

Fig. 2. (a) Simplified geological map of French Guyana (modified after Ledru et al. (1991)); (b) Geological map of the Oyapok and Camopi rivers zone (modified after Marot (1988)). Sampling location for paleomagnetic and geochronological studies are indicated.

2.2. Paleomagnetic and geochronological sampling

Paleomagnetic samples were collected in 16 sites along the Oyapok and Camopi rivers (Fig. 2 and Table 1) from tonalite (five sites), amphibolites and metasediments (ten sites) and from meta-ultrabasites (one site). The tonalite has a coarse-grained texture and is composed of magnesiohornblende, biotite, plagioclase (An_{30}–An_{60}), interstitial quartz and titanite as the principal accessory minerals. In each site, six or seven cores were drilled. Core orientation was measured by magnetic compass and, whenever possible, by sun orientation. The average difference between solar and magnetic azimuth measurements is about 18±2°, which is compatible with the 1998 IGRF declination (17.5°) for this location. Cores were cut to standard size (2.54/2.2 cm), yielding about 100 specimens. Two sites were sampled for the geochronological investigation. One corresponds to the paleomagnetic site GN and, in order to constrain the cooling rate, another (B107) was sampled 20 km farther north in a separate pluton (Fig. 2).

Table 1. Summary of paleomagnetic sampling and analysis results. Slat. and Slong.: latitude and longitude of the site; Dec., Inc., k, α_{95} (A_{95}): declination, inclination, precision parameter and confidence interval at the 95% level; n/N: number of entries in statistics/number of treated specimens; Plat. and Plong.: latitude and longitude of polar coordinatesa

Site	Rock	Slat.	Slong.	n/N	Dec.	Inc.	Plat.	Plong.	k[a]	α_{95}	A_{95}
Paramaca rocks											
GC	amphibolite	2° 59′ 42″	−52° 21′ 58″						scattered		
GE	metasediment	3° 10′ 33″	−52° 29′ 10″	4/7	15.9°	26.7°			17.3	15.3°	
GF	metasediment	3° 12′ 43″	−52° 27′ 22″	3/6	339.6°	19.9°			10.3	30.0°	
GG	amphibolite	3° 13′ 00″	−52° 23′ 49″						scattered		
GI	amphibolite	3° 12′ 13″	−52° 24′ 24″						scattered		
GJ	metasediment	3° 12′ 59″	−52° 23′ 50″						scattered		
GK	metasediment	3° 10′ 45″	−52° 20′ 02″	4/6	348.3°	38.7°			13.5	26.0°	
GL	amphibolite	3° 10′ 35″	−52° 21′ 55″						scattered		
GM	amphibolite	3° 07′ 17″	−52° 20′ 54″	4/7	348.1°	26.2°			16.5	15.3°	
GP	amphibolite	3° 13′ 13″	−52° 17′ 37″	4/6	339.1°	3.4°			10.5	29.8°	
Means				5/10	348.9°	26.6°			18.7	18.2°	
Meta-ultrabasite and tonalite											
GH	Meta-ultrabasite	3° 12′ 34″	−52° 26′ 38″	6/6	157.9°	54.4°	−46°	334.5°	177.3	4.1°	
GN	tonalite	3° 08′ 07″	−52° 20′ 47″	7/8	136.0°	56.6°	−33°	349.9°	33.5	9.5°	
PQ	tonalite	3° 08′ 10″	−52° 20′ 41″	6/6	120.2°	63.0°	−19°	348.8°	28.9	9.7°	
PR	tonalite	3° 08′ 27″	−52° 20′ 36″	5/6	137.2°	67.6°	−26°	336.8°	58.8	7.9°	
PS[b]	tonalite	3° 08′ 34″	−52° 20′ 27″	6/6	330.0°	75.2°	−27°	292.6°	70.2	5.0°	
PT	tonalite	3° 08′ 40″	−52° 20′ 14″	6/7	116.2°	54.7°	−19°	358.7°	60.5	7.8°	
Means OYA				5/6	133.8°	60.2°			59.9	9.9°	
							−28.0°	346.0°			13.8°

[a] 'Scattered' indicates a non-Fisherian distribution.
[b] Site excluded from mean calculation.

3. Laboratory measurements and analytical procedures

3.1. Magnetic mineralogical analysis and petrographic study

To characterize magnetic mineral compositions, we applied the following methods on representative samples: reflection microscopy (Olympus BX60) at the geological laboratory of Université d'Orléans; scanning electronic microscopy (SEM, JEOL) at Ecole Supérieur de l'Energie et des Matériaux (ESEM) in Orléans; thermomagnetic experiments using a CS3 apparatus coupled with a KLY-3S kappabridge (AGICO, Geofysica) at the joint BRGM/Université d'Orléans Laboratoire de Magnétisme des Roches (LMR). Isothermal remanent magnetization was measured with an IM-10 impulse magnetizer and a JR5 spinner magnetometer (AGICO, Geofysica), and the latter was also used for remanent magnetization measurements. Hysteresis loops were realized with a translation inductiometer within an electromagnet providing a field of up to 1.5 T at the Paleomagnetic Laboratory of Saint Maur (Paris).

3.2. $^{40}Ar/^{39}Ar$ analytical procedures

$^{40}Ar/^{39}Ar$ ages were measured at the geochronological laboratory of Nice. Single grains of biotite and amphibole were separated by heavy liquids and finally isolated by hand picking (in BRGM). They were carefully selected under a binocular microscope from the coarser fractions. Grain sizes varied from 200 to 400 μm. The samples were irradiated at McMaster Nuclear Reactor in the University of Hamilton, Canada, with total flux of 3×10^{18} n cm^{-2}. The maximum flux gradient is estimated at ±0.2% in the volume where the samples were included. The irradiation standard was the Hb3gr hornblende as a flux monitor with age of 1072 Ma (Turner et al., 1971; recently confirmed by Renne, 2000). The classical step-heating procedure is described by F and F and performed with a laser probe using a Coherent Innova 70-4 continuous argon-ion laser model. The mineral was located on a copper sample-holder,

beneath a Pyrex window. Each step-heating laser experiment lasted about 4 min: 1 min of laser heating, 2 min of clean-up in the purification line, consisting of a getter operating at 400°C and an N_2 cold trap, and finally 40 s of inlet time into the mass spectrometer. The temperature is not known, but its homogeneity was controlled by binocular microscope coupled with a color video camera and recorder. The mass spectrometer was a VG3600 working with a Daly detector system. Isotopic measurements were corrected for K, Ca and Cl isotopic interferences, mass discrimination, and atmospheric argon contamination. The measured $^{40}Ar/^{39}Ar$ atmospheric ratio, determining the mass discrimination, was 289.3±1 during the analyses.

To define a plateau age, at least three consecutive steps are needed, corresponding to a minimum of 70% of total $^{39}Ar_K$ released, and the individual fraction ages should agree within 2σ with the 'integrated' age of the plateau segment. All uncertainties are quoted at the 2σ (except the apparent ages in Table 2 and age spectra, which are given at the 1σ level) and do not include the uncertainties on the age of the monitor. The uncertainties on the $^{40}Ar^*/^{39}Ar_K$ ratios of the monitor are included in the calculation of the plateau age uncertainty.

Table 2. Detailed $^{40}Ar/^{39}Ar$ analytical results. $^{40}Ar^*$: radiogenic ^{40}Ar; Ca and K: produced by Ca and K neutron interference, respectively. Decay constants are those of Steiger and Jäger (1977). Correction factors for interfering isotopes were $(^{39}Ar/^{37}Ar)_{Ca}=7.06\times10^{-4}$, $(^{36}Ar/^{37}Ar)_{Ca}=2.79\times10^{-4}$, $(^{40}Ar/^{39}Ar)_{K}=2.97\times10^{-2}$. Data given in italics are excluded from the age calculation for GN

Laser step (mV)	Atmospheric (%)	$^{39}Ar_K$ (%)	$^{37}Ar_{Ca}/^{39}Ar_K$ (%)	$^{40}Ar^*/^{39}Ar_K$ (%)	Age (Ma)
B107 amphibole					
59	12.10	0.04	14.89	645.63	5768.14 ± 358.96
157	1.03	2.46	3.69	66.17	2210.43 ± 10.69
169	0.00	3.53	3.67	59.11	2069.15 ± 10.39
177	1.58	6.39	3.72	57.33	2031.59 ± 32.45
189	0.01	11.47	3.74	58.42	2054.71 ± 3.78
198	0.01	39.27	3.72	58.36	2053.47 ± 2.73
208	0.22	5.41	3.70	58.33	2052.67 ± 7.95
228	0.00	6.30	3.70	58.47	2055.68 ± 7.68
287	0.55	5.36	3.72	57.67	2038.76 ± 8.42
Fuse	0.13	19.78	3.70	58.17	2049.39 ± 3.96
Total age:					2065.39 ± 4.40
B107 biotite					
18	61.90	1.25	0.09	19.99	985.48 ± 28.27
30	1.38	6.07	0.00	50.75	1885.96 ± 4.54
35	0.15	12.36	0.01	54.28	1965.56 ± 2.69
38	0.00	13.56	0.01	55.65	1995.59 ± 3.12
41	0.03	5.63	0.01	55.68	1996.16 ± 3.67
48	0.00	4.82	0.01	56.09	2005.05 ± 4.71
55	0.00	6.56	0.01	56.00	2003.18 ± 3.87
59	0.00	4.74	0.02	55.56	1993.55 ± 4.61
63	0.00	5.76	0.01	55.52	1992.68 ± 3.75
68	0.00	3.89	0.01	55.10	1983.57 ± 5.67
77	0.00	4.96	0.03	55.01	1981.67 ± 4.71
89	0.00	2.29	0.00	55.77	1998.08 ± 14.42
109	0.36	3.92	0.00	55.05	1982.37 ± 19.40
149	0.00	14.72	0.00	55.47	1991.53 ± 2.76
159	0.32	3.15	0.00	56.27	2008.85 ± 6.51
190	0.00	5.50	0.00	56.09	2005.04 ± 4.37
Fuse		0.79	0.05	56.61	2016.20 ± 13.52
Total age:					1975.31 ± 1.32
GN amphibole					
91	42.8	0.24	0.00	190.26	3732.22 ± 33.23
220	6.33	0.54	0.00	80.81	2472.39 ± 25.71
350	3.03	1.84	0.23	81.71	2487.22 ± 8.30
370	1.47	0.78	0.82	59.91	2085.75 ± 16.08
405	0.84	1.09	0.00	57.86	2042.89 ± 14.45
450	0.74	2.05	1.08	57.27	2030.38 ± 7.41
500	0.00	3.41	2.4	56.85	2021.39 ± 4.91
542	0.04	14.23	3.80	56.61	2016.18 ± 2.86
557	0.03	13.57	3.82	56.81	2020.55 ± 2.86
567	0.36	5.80	4.07	56.18	2006.97 ± 4.18
593	0.17	6.80	4.01	56.81	2020.47 ± 3.22
636	0.27	15.79	4.39	57.07	2026.14 ± 2.72
669	1.74	1.62	3.31	55.87	2000.23 ± 10.66
748	0.49	6.42	4.12	56.78	2019.85 ± 3.73
548	0.62	2.59	4.32	55.92	2001.35 ± 8.14
1048	0.28	8.43	4.79	57.19	2028.55 ± 2.97
Fuse	0.19	14.8	4.43	56.94	2023.35 ± 2.59
Total age:					2040.52 ± 1.00

Table 2 (*Continued*)

Laser step (mV)	Atmospheric (%)	$^{39}Ar_K$ (%)	$^{37}Ar_{Ca}/^{39}Ar_K$ (%)	$^{40}Ar^*/^{39}Ar_K$ (%)	Age (Ma)
GN biotite					
25	79.76	0.14	0.00	36.33	1518.60 ± 91.34
38	57.77	0.12	0.00	33.56	1438.43 ± 81.93
83	30.54	0.90	0.00	34.92	1478.41 ± 17.17
103	15.67	2.05	0.01	52.41	1923.94 ± 6.29
113	2.56	4.41	0.00	54.30	196591 ± 3.42
118	1.20	4.28	0.00	54.54	1971.19 ± 3.22
123	1.15	3.30	0.00	54.75	1975.94 ± 3.57
139	0.80	4.14	0.01	54.74	1975.70 ± 4.21
155	*0.41*	*4.18*	*0.01*	*53.12*	*1984.00 ± 0.00*
170	*0.45*	*4.72*	*0.01*	*54.99*	*1981.23 ± 3.19*
185	0.43	3.33	0.00	54.48	1969.89 ± 4.36
215	0.25	6.02	0.00	54.74	1975.75 ± 2.85
238	0.44	5.38	0.01	54.54	1971.25 ± 3.25
253	0.18	4.06	0.00	54.67	1974.08 ± 3.28
270	0.30	3.91	0.00	54.83	1977.73 ± 3.60
290	0.13	5.18	0.00	54.64	1973.45 ± 2.67
309	0.27	3.83	0.00	54.53	1971.07 ± 4.43
335	0.12	10.69	0.00	54.55	1971.57 ± 3.25
343	0.00	3.80	0.00	54.82	1977.45 ± 3.40
356	0.22	2.98	0.00	54.68	1974.32 ± 4.35
378	0.31	3.69	0.00	54.48	1969.89 ± 3.10
418	0.38	4.71	0.00	54.56	1971.71 ± 3.37
495	0.05	6.28	0.00	54.63	1973.29 ± 2.85
591	0.35	4.96	0.00	54.59	1972.49 ± 3.50
Fuse	0.59	2.18	0.02	54.54	1971.38 ± 6.28
Total age:					1967.76 ± 0.79

4. Magnetic mineralogy

Petrographic observations in transmitted light show a considerable amount of subautomorphous grains of magnetite (Fig. 3a), with xenomorphous grains of ilmenite, pyrite in tonalite and meta-ultrabasite. However, in Paramaca rocks, elongate ilmenite consists of the principal ferri-oxide and no magnetite grains were observed (Fig. 3b). The saturation field for isothermal remanent magnetization (IRM) is 0.3 T (Fig. 4a) for tonalitic rock. The magnetic saturation intensity for tonalite samples is greater than 30 A m^{-1} (Fig. 4a). Thermomagnetic curves show sharp drops for tonalite and meta-ultrabasite rocks at around 560–580°C (samples GN4 and GH1, respectively; Fig. 4b), and do not show a drop for the Paramaca (samples GM4; Fig. 4c). Hysteresis loops performed on the tonalite rocks showed narrow-waisted and typical low coercivity magnetite grains (Fig. 4d; Raposo and D'Agrella-Filho, 2000). In contrast, the Paramaca samples presented hysteresis curves of a perfectly linear superposition of induced magnetic moment by increasing and decreasing magnetic fields (Fig. 4e), indicating the strong dominance of the paramagnetic minerals in these rocks.

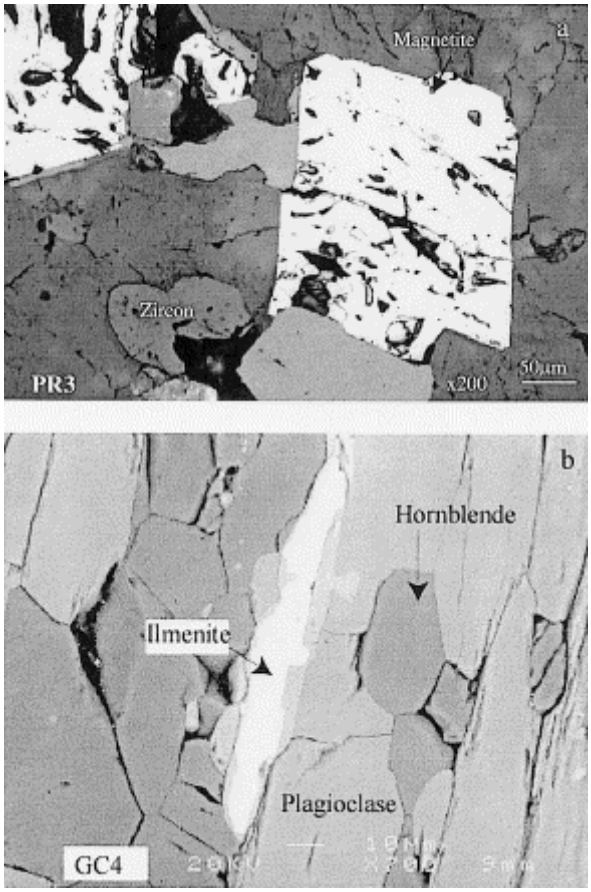

Fig. 3. (a) Reflected light photograph of a large subautomorphous titanomagnetite grain in tonalite from site GN. (b) Large-scale image in secondary electrons (SEM) of ilmenite from site GC4.

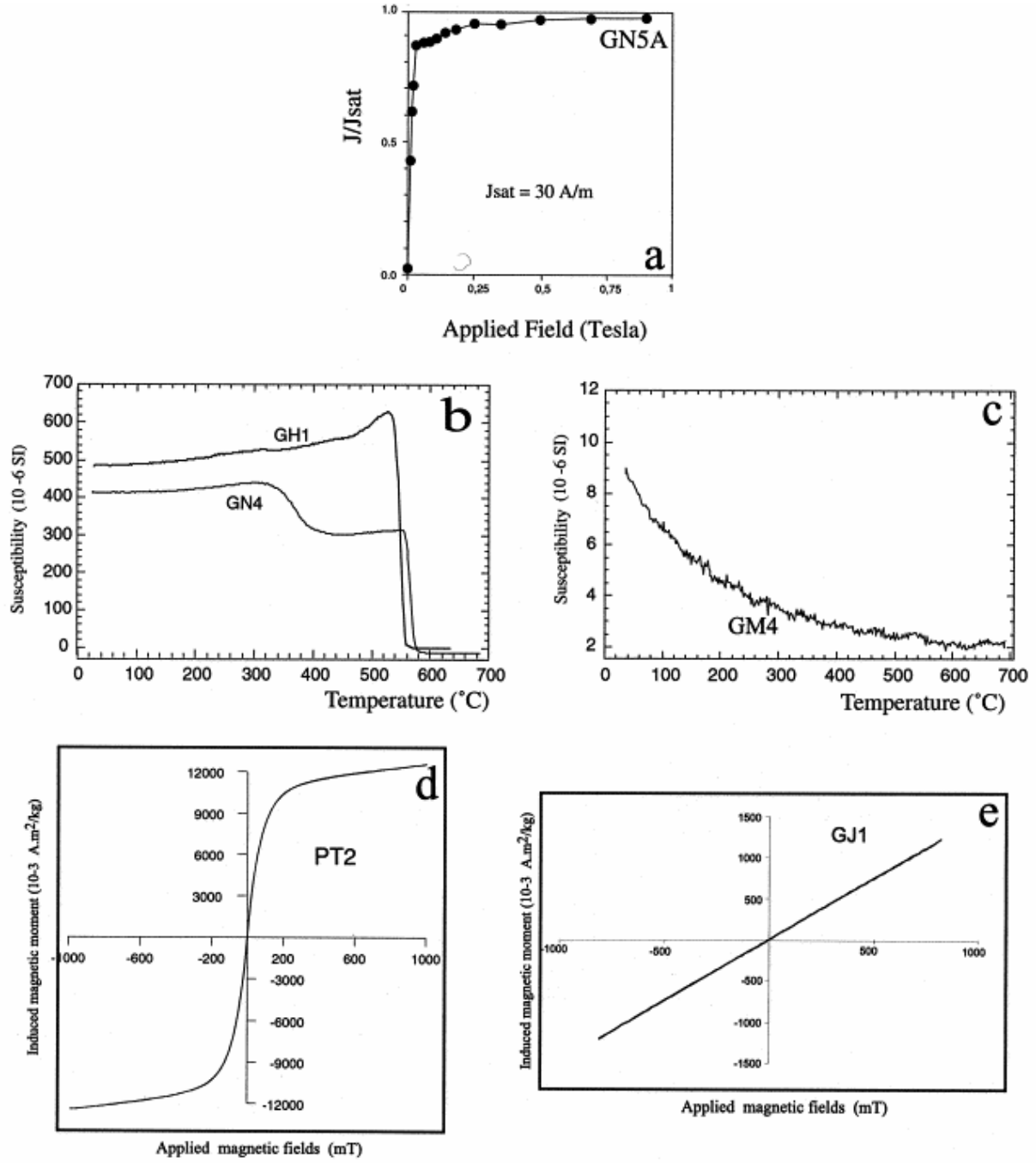

Fig. 4. Typical isothermal remanent magnetization (IRM) acquisition for tonalite and meta-ultrabasite rocks (a). Typical curves of the thermomagnetic experiments for the tonalite, meta-ultrabasite (b) and Paramaca rocks (c). Hysteresis curves performed on the tonalite rocks showing a narrow-waisted and typical of low coercivity magnetite grains (d) and (e) Paramaca rocks showing a perfectly linear superposition of the two induced magnetic moment curves produced by increasing and decreasing magnetic fields.

The above observations suggest that the magnetite is the principal ferromagnetic mineral in tonalite and meta-ultrabasite and the total absence of ferromagnetic minerals in Paramaca rocks, or very weak concentration of magnetite.

5. Paleomagnetic results

A pilot study was carried out on several specimens using both thermal and alternating magnetic field (AF) demagnetizations with a Pyrox furnace and an automated three-axis tumbler AF demagnetizer (LDA-3, AGICO geofysica), respectively. About 10 (AF, 1 to 100 mT) to 15 (thermal, ~20 to 595°C) progressive steps were applied to the demagnetization procedure.

5.1. Paramaca

Amphibolites and metasediments presented unimodal NRM intensities and susceptibilities ranging from 0.1 to 10 mA m^{-1} and 2 to 7×10^{-4} SI, respectively. Most of the Paramaca rocks were treated with the AF demagnetization method because of the unstable magnetic behavior during thermal treatment. A typical demagnetization response of these rocks is plotted in Fig. 5a. Initially, the magnetic remanence decays linearly until about 8 mT, then the direction becomes random and no characteristic component could be isolated from higher fields. Moreover, this low coercive magnetization could be observed only in five out of ten Paramaca sites, and directional analyses using the principal component analysis (Kirschvink, 1981) show dispersed directions within each site with poor statistical parameters (Table 1; Fisher, 1953). A mean direction was calculated from five sites: Dec=349.8°, Inc=23.6°, k=18.7 and α_{95}=18.2°, which is not significantly different from the present Earth field (D=342.5°, I=18.5°, Fig. 6a). As described in the Section 4, no magnetite grains were found and the viscous behavior of these samples precludes any further discussion.

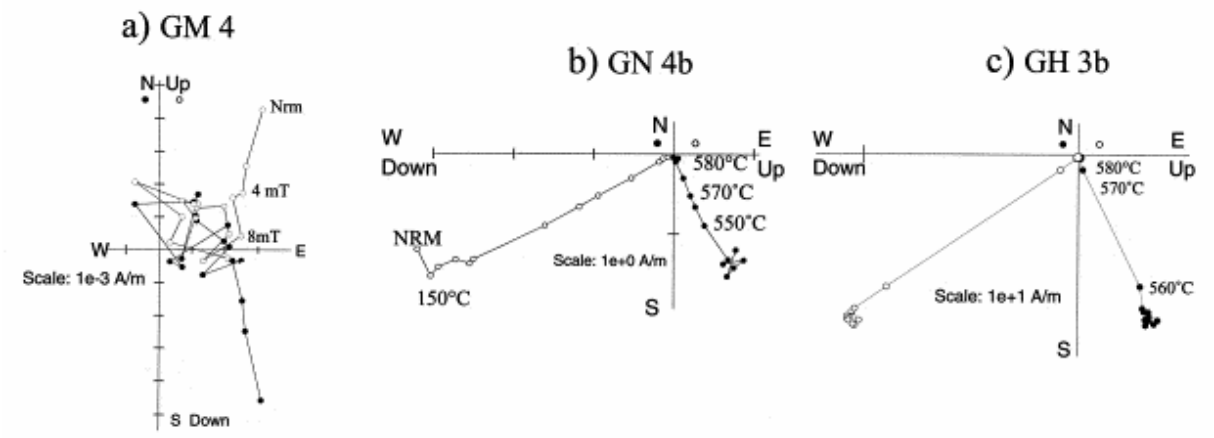

Fig. 5. Representative orthogonal vector diagrams (Zijderveld, 1967) of progressive thermal and alternating field demagnetizations. The closed (open) symbol refers to the horizontal (vertical) plane. (a) Low coercive remanent direction in Paramaca. (b) and (c) Typical SE declinations with medium to high positive inclinations for tonalite and meta-ultrabasite rocks.

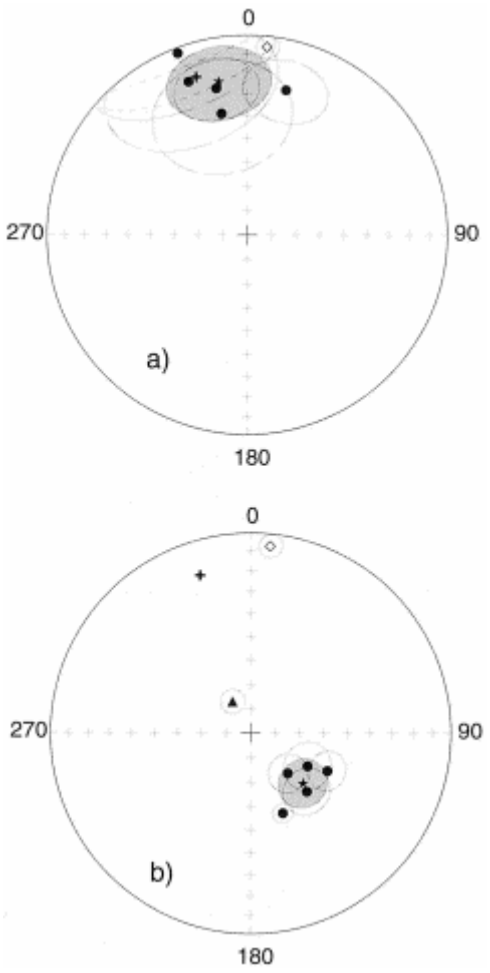

Fig. 6. Equal-area stereoplot of mean direction: (a) Paramaca; (b) tonalite and meta-ultrabasite. The star stands for the mean direction with corresponding 95% confidence oval, cross for the present Earth field and diamond shape for local Early Jurassic pole (Nomade et al., 2000). The triangle represent the mean direction of site PS (excluded from the average).

5.2. Tonalite and meta-ultrabasite rocks

NRM intensities vary from 100 to 800 mA m^{-1} and susceptibilities range from $9\times10-^{4}$ to 2×10^{-2} SI. They were thermally treated because complete demagnetization of NRM could be achieved. The representative results are plotted in orthogonal vector diagrams (Zijderveld, 1967) (Fig. 5b and c). For both tonalite and meta-ultrabasite rocks, after the removal of a low unblocking temperature random component at ~150°C (Fig. 5b), the direction becomes stable. The remanence is unblocked above 540°C and decays linearly to the origin until 580°C. The characteristic directions, namely OYA, are dominated by moderately steep downward inclinations with south-eastward declination, except for site PS. The magnetic directions within each site are well grouped, and thus mean directions are computed by Fisher statistics (Fig. 6b, Table 1). The mean directions are distinct from the present Earth's field and the geocentric axial dipole field. The Fisher parameter k is usually greater than 30 with α_{95} less than 10° (Table 1). These directions are also distinct from the local Early Jurassic dike paleomagnetic components characterized by a north-eastward declination and low inclination (Fig. 6b, Nomade et al., 2000). The above observations and the presence of subautomorphous magnetite grains with no evidence of a later destabilization (see Section 4) suggest that the magnetic remanence is of primary origin and represents a Paleoproterozoic magnetization.

Site PS was sampled in the middle of the Oyapok River on a very limited outcrop. This outcrop was perhaps not in situ and could be a free block. Therefore, this site was excluded from the mean direction calculation: Dec=133.8°, Inc=60.2°, k=59.9, α_{95}=9.9° and N=5 (Fig. 6b). The corresponding virtual geomagnetic pole (VGP) is OYA: λ=28.0°S, φ=346.0°E, k=31.9, A_{95}=13.8° and N=5 (Table 1).

6. $^{40}Ar/^{39}Ar$ results

Analytical data for four dated specimens are given in Table 2. Fig. 7 shows age and $^{37}Ar_{Ca}/^{39}Ar_K$ ratio spectra for minerals from B107 (Fig. 7a and b) and site GN (Fig. 7c and d).

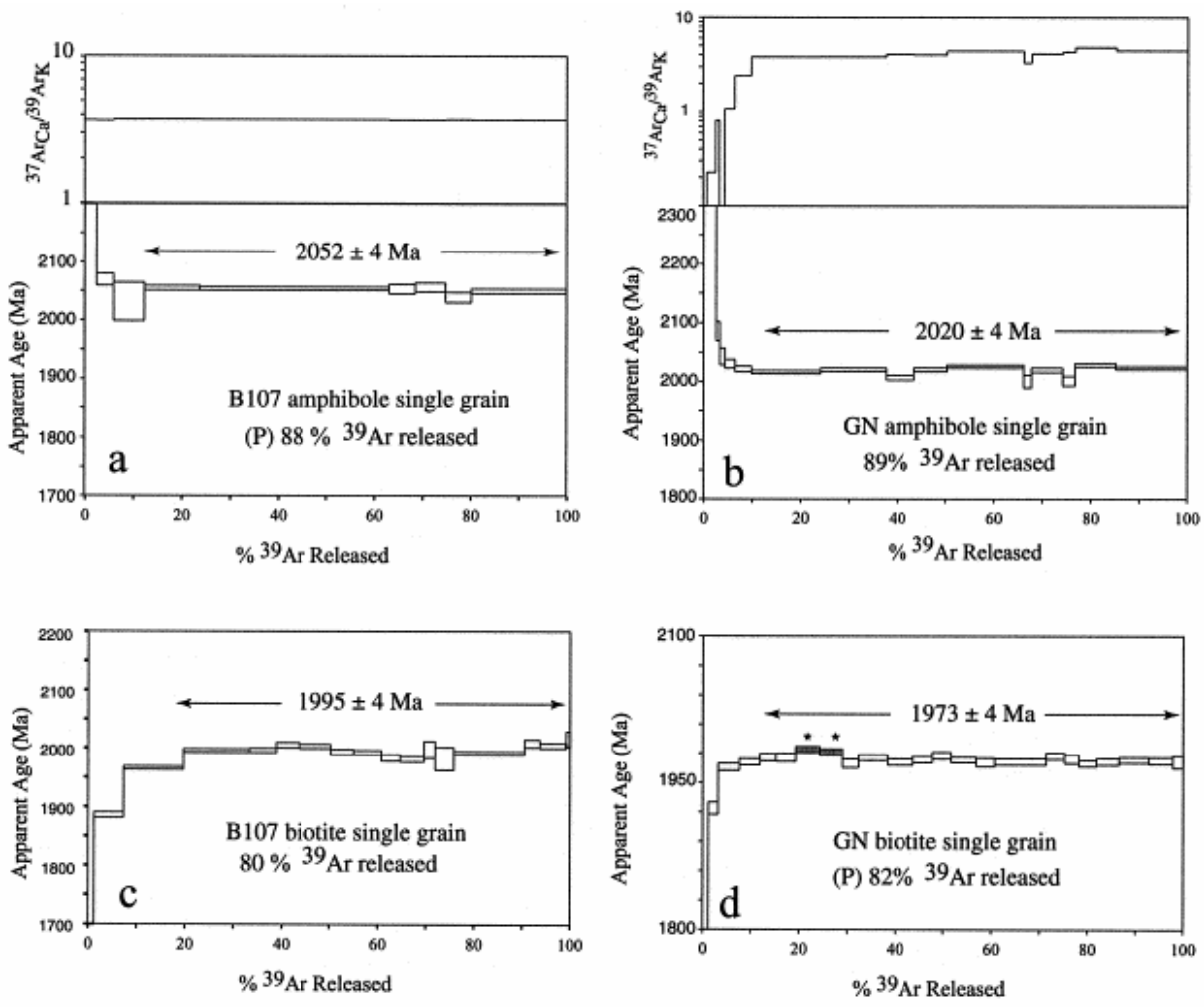

Fig. 7. $^{40}Ar/^{39}Ar$ age spectra for amphibole and biotite from tonalite (a and c for B107 sample; b and d for the tonalite of the paleomagnetic site GN). $^{40}Ar_{Ca}/^{39}Ar_K$ ratio spectra displayed by amphiboles are also shown. P indicates plateau ages. * Indicates the steps probably affected by ^{39}Ar recoil due to slight chloritization of biotite, and excluded from the plateau age calculation.

Amphibole single grains (green grains) yield a very flat spectrum for the B107 and GN specimens (Fig. 7a and b), after a sharp decrease in age at low temperature. The corresponding $^{37}Ar_{Ca}/^{39}Ar_K$ ratios remain constant throughout the flat section of spectra (Fig. 7a and b) and indicate that pure amphiboles were analyzed. The plateau age is 2052±4 Ma (88% ^{39}Ar released) for B107. The GN specimen does not show a plateau age following our

criteria defined above. The flatness of the spectrum on more than 90% of ^{39}Ar leads us to interpret the corresponding weighted mean age with 93% ^{39}Ar released of 2020±4 Ma as reliable.

Biotite single grains display age spectra (Fig. 7c and d) characterized by (1) a sharp increase of age at low temperature followed by a more or less flat section over at least 80% of ^{39}Ar released. In the case of B107, this section is characterized by a slight increase of ages (step 6–7) followed by a decrease. This is typical of slightly chloritized biotites affected by ^{39}Ar recoil during irradiation (Ruffet et al., 1991). It is therefore likely that the weighted mean of 1995±4 Ma, calculated on 80.3% ^{39}Ar, is reliable. For the GN biotite age, the very flat section over 87% of ^{39}Ar (19 steps) is only altered by two steps (9 and 10) that are clearly the results of slight ^{39}Ar recoil. Therefore, we calculated a plateau age of 1973±4 Ma with 17 steps excluding the discordant steps 9 and 10.

7. Discussion

7.1. Age of the magnetic remanence

The significant difference of 47 Ma in $^{40}Ar/^{39}Ar$ ages observed in amphiboles and biotites for site GN in the central Oyapok zone shows that the GN tonalite rock cooled down from about 500–550°C to about 250–350°C at about 2020±4 Ma and 1973±4 Ma, respectively, according to the proposed biotite and amphibole K/Ar blocking temperatures (Harrison and Harrison). It is important to notice that the compositional effect in hornblende K/Ar closure temperature (Dahl, 1996) suggests a temperature of 500±5°C for Mg-rich amphibole. Nevertheless, this high precision isotopic closure temperature is not adequate because of the many uncertain factors that can be induced by K diffusion in amphibole. For the biotite the compositional effect in closure temperature is well documented by Grove and Harrison (1996), but this effect is unpredicted and does not allow the constraint of the uncertainties in the isotopic closure temperature. For these reasons, we have used the blocking temperatures proposed above (Harrison and Harrison).

A similarly important difference in ages (57 Ma) between these two minerals is also displayed in a separate pluton (B107 specimen; 2052±4 Ma and 1995±4 Ma, for amphiboles and biotites respectively), suggesting that low cooling rate was homogeneous during the Paleoproterozoic in this zone.

The magnetic remanence was acquired by the magnetite grains during the protracted cooling of the intrusion. The age of magnetization must, therefore, lie between the crystallization age of the rocks and the ($^{40}Ar/^{39}Ar$) biotite age 1973±4 Ma in site GN. $^{40}Ar/^{39}Ar$ data are plotted on a *T*/*t* diagram (Fig. 8) in order to estimate tentatively the magnetic remanence age for the pole OYA. A relatively slow cooling rate of 4.8+2.6/−2.1°C Ma^{-1} is deduced from these ages. Despite the possible bias between K/Ar and Pb/Pb ages due to a poor precision on the ^{40}K decay constants (Min et al., 2000), we plotted the Pb/Pb ages of the French Guyana plutonic activity (Pb/Pb ages, Vanderhaeghe et al., 1998; Fig. 8). This rate is in agreement with a low unpredictable rate starting between 2130 and 2080 Ma (<800°C, Lee and Dahl). This cooling rate is in agreement with that from greenstone-belt granites of similar age in the São-Fransisco craton (Chauvet et al., 1997) and can be interpreted as the result of gradual exhumation. By using magnetic blocking temperatures between 540 and 580°C, which corresponded to the unblocked temperatures of our samples (see above), we obtain for site GN a magnetic remanence age of 2036±14 Ma for the pole OYA.

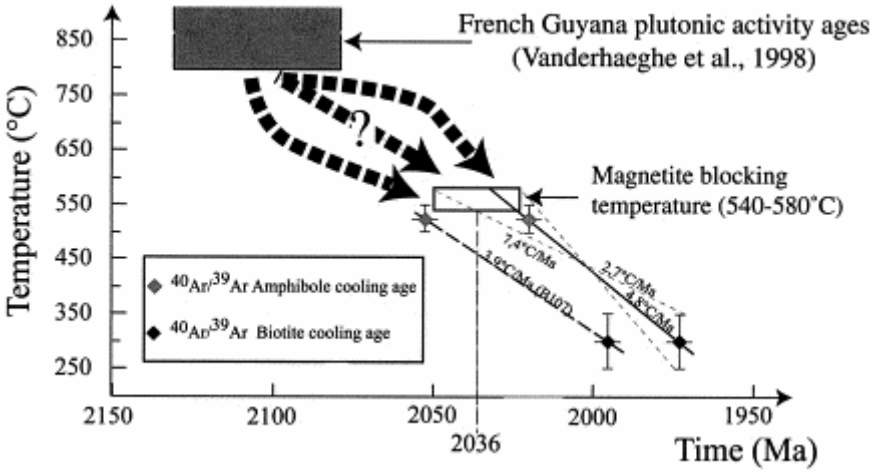

Fig. 8. Temperature–time diagram showing the inferred cooling paths for the two sampling zones: B107 in dotted line and GN in solid line. Previous Pb/Pb geochronological investigations for French Guyana (Vanderhaeghe et al., 1998) are also indicated.

7.2. Paleogeographic and geodynamic implications

The new paleomagnetic pole (OYA) from French Guyana and available Paleoproterozoic paleomagnetic data from the nearby zone (Venezuela) of the Guyana Shield are listed in Table 3. The results from Imataca granulite (Im 1 and Im 2; squares in Fig. 9a) and Encrucijada granite (En A1 and En A2; circles in Fig. 9a) show consistent poles and Rb/Sr ages, with due consideration of statistical errors (Fig. 9a). This suggests that the GFZ has experienced no significant activity since 2000 Ma from the point of view of paleomagnetism. Therefore, a mean pole for this area was calculated (Table 3, Fig. 9a). Fig. 9a shows that pole OYA is statistically distinct from the other four poles from Venezuela, and from their mean poles with an angular difference of 32.6±21.5°. The difference between these two poles reflects a paleolatitudinal difference (31.8±21.5°) with consistent declinations (0.6±23.9°). Two hypotheses may be proposed to explain this difference: (i) if the ages of magnetic remanence are similar among the paleomagnetic data, over 1000 km of latitudinal crustal shortening had occurred between the Venezuela and French Guyana blocks separated by the PJF since that age (relative movement); (ii) if the magnetic remanence ages of these two blocks are different, the same order of latitudinal displacement of the blocks occurred during the corresponding period (absolute movement).

Table 3. Available Paleoproterozoic poles for the Guyana Shield and their possible paleomagnetic corresponding ages. Plat. and Plong.: latitude and longitude of polar coordinates; N, α_{95}, Lat.: number of site, confidence interval at 95% level, paleolatitude

Rock		Plat.	Plong.	α_{95}	N	Lat.	Methode of dating	Magnetie remanence age (Ma)	Reference
OYA	(tonalite, meta-ultrabasite)	−28.0°	346.0°	13.8°	5	41°S	$^{40}Ar/^{39}Ar$ Amph: 2020 ± 4 Ma; $^{40}Ar/^{39}Ar$ Biot: 1973 ± 4 Ma	2036 ± 14	This study
Im 1	granulite	−49.0°	18.0°	18.0°	3	10°S	Rb/Sr isochron:2020 ± 60 Ma (Montgomery and Hurley, 1978)		Onstott and Hargraves (1981)
Im 2	granulite	−29.0°	21.0°	18.0°	3	13°S			
En A1	granite	−55.0°	8.0°	6.0°	5	1°S	Rb/Sr isochron: 2064 ± 87 Ma; $^{40}Ar/^{39}Ar$ Amph: 1972 ± 4 Ma; $^{40}Ar/^{39}Ar$ Biot: 1882 ± 2 Ma		
En A2	granite	−37.0°	36.0°	18.0°	3	14°S		2000 ± 10	Onstott et al. (1984)
Mean of Venezuela poles		43.0°	22.0°	16.5°	4	9°S			

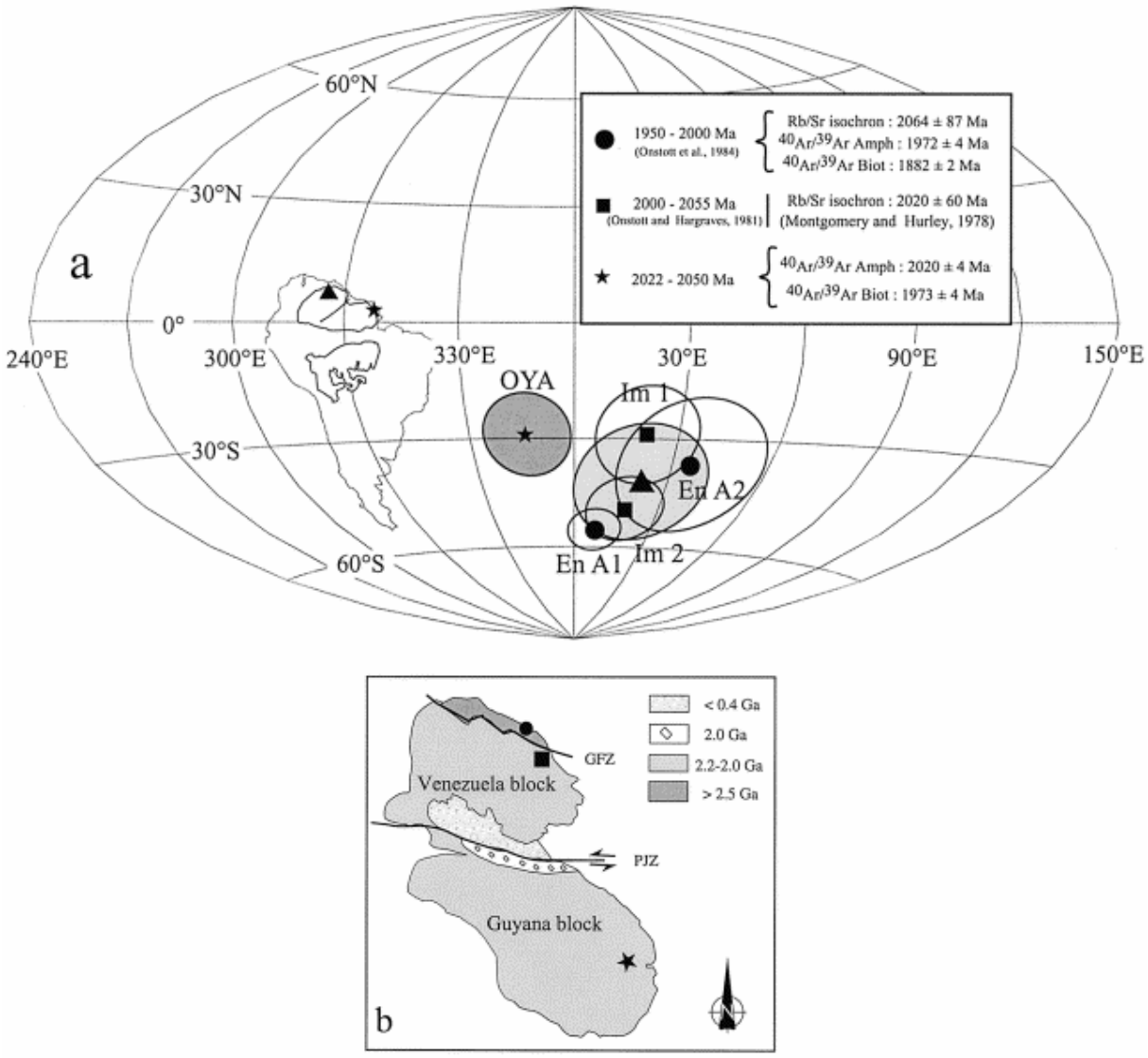

Fig. 9. (a) Aitoff Hammer projection of the paleomagnetic poles from the present study (star) and Venezuela (triangle) (Onstott and Hargraves, 1981 (square); Onstott et al., 1984 (circle)). (b) The Paleoproterozoic orientation of the Guyana Shield with respect to the paleo-north.

The Rb/Sr dating method was applied to both Imataca granulite and Encrucijada granite and yielded concordant ages of 2020±60 Ma and 2062±87 Ma (Onstott; Onstott and Onstott). The new age of pole OYA (2036±14 Ma) is included within the statistical estimates of the previous two, but the statistical precision is too poor (>60 Ma) to determine whether these ages are really consistent. However, the Encrucijada granite was also dated by the $^{40}Ar/^{39}Ar$ method on biotite and amphibole, which show two ages of 1975±4 Ma and 1882±2 Ma (1σ) respectively. Onstott et al. (1984) demonstrated that the isolated magnetic components from Encrucijada granite were carried by magnetite grains. In order to estimate the magnetization age for Encrucijada granite, we used similar isotopic and magnetic temperature closures for the amphibole, biotite and magnetite as described above. The magnetization age for the Encrucijada pluton was found to be 2000±10 Ma (Table 3) with an estimated cooling rate of ca 2±1°C Ma^{-1} (Swapp and Onstott, 1989). This age appears significantly different from that of pole OYA (about 36±16 Ma). The difference of about 1.6% in age between these two groups of paleomagnetic data is significant because the two series of minerals were irradiated with the same flux monitor Hb3gr, which is appropriate for this age domain, and in the same nuclear reactor.

Geographically, the two paleomagnetic sampling zones (Venezuela and French Guyana) are separated by the senestral PFZ (Fig. 1 and Fig. 9b) and the CGGB. The age of granulitization for the core of the Falawatra complex part in the CGGB in Suriname was estimated between 2006 to 2046 Ma (U/Pb, Bosma et al., 1983). According to these paleomagnetic data the paleogeographical reconstruction indicates that these fault zones had a nearly east–west orientation at about 2.0 Ga (Fig. 9b). Therefore, the possible longitudinal displacement along this mobile zone between the two blocks at that time cannot be detected by paleomagnetism. Moreover, no high-pressure metamorphism (<8 kbar) and/or important shortening are known in the CGGB zone separating the two blocks (Kroonenberg, 1976).

Based on geological and geochronological data, the 31.8±21.5° latitudinal difference between the French Guyana block at 2036±14 Ma and Venezuela block at 2000±10 Ma may correspond to a northward movement (in respect of the pole polarity proposed by Onstott et al. (1984)) of the Guyana Shield from 40°S to 10°S. The rate of this northward displacement is estimated as 9±7 cm/year, which is similar to present high-velocity plate movement.

8. Conclusion

The paleomagnetic and geochronological data from this and previous studies lead to the following conclusions.

(1) Subautomorphous magnetite is the principal magnetic remanence carrier for tonalite and meta-ultrabasite from our sample collection. In the majority of the greenstones (Paramaca formation) the ferromagnetic minerals are rare or absent.

(2) Two magnetic components were obtained, one from the Paramaca rock (P) and one from tonalite, meta-ultrabasite rocks (OYA). Unstable Paramaca magnetic components reflect a viscous overprint of recent origin. We found that component OYA is of primary origin and represents a Paleoproterozoic magnetization. Pole OYA was therefore computed from OYA components: λ=28.0°S, φ=346.0°E, k=31.9 and A_{95}=13.8° and N=5.

(3) $^{40}Ar/^{39}Ar$ results show systematic and similar differences between amphibole and biotite ages on two dated rocks; the slow cooling rate of ca 4.8+2.6/−2.1°C Ma^{-1} of the rocks was

interpreted between about 525 and 300°C as being due to the gradual exhumation of the Oyapok–Camopi river zone. A magnetization age of 2036±14 Ma from tonalite and meta-ultrabasite was extrapolated from this slow cooling rate.

(4) The new paleomagnetic pole OYA from French Guyana is significantly distinct in latitude from that of Venezuela (Encrucijada pluton), with an estimated magnetization age of 2000±10 Ma. This difference of 1.6% in age between the two blocks is probably significant and may be the result of a northward movement of the Guyana Shield of 31.8±21.5° from about 2036 to 2000 Ma with an estimated rate of 9±7 cm/year.

(5) Relative movement between the French Guyana and Venezuela blocks along the Pisco Jurua fault zone cannot be estimated during this period by paleomagnetic investigations owing to the east–west orientation of this mobile zone during the 2036–2000 Ma period.

Acknowledgements

This study was supported by the French geological survey (BRGM) French Guyana mapping project and by a French region Centre PhD grant. Dr P. Rossi, Dr C. Delors, Dr D. Lahondere, Dr M.T. Lins Faraco, Dr J.M. Carvalho, Dr O. Monod, and Dr M. Vidal are thanked for their contribution in sampling and discussions. The constructive suggestions proposed by J. Meert and I.G. Pacca are very much appreciated for improving the manuscript. We also thank B. Henry and M. Le Goff for their help in hysteresis loop measurements, N. le Breton and A. Lacour for their help in microscopic petrographic verifications, R.J. Enkin, J.P. Cogné and Y. Ageon for the use of their paleomagnetic and argon software, as well as Dr A. Mort for the language improvement of the manuscript and P. Jézequel for mineral separation.

References

Berger, G.W., 1979. Calibration of Grenvillian paleopoles by $^{40}Ar/^{39}Ar$ dating. *Nature* **277**, pp. 46–47.

Bosma, W., Kroonenberg, S.B., Mass, K. and De Roever, E.W.F., 1983. Igneous and metamorphic complexes of the Guiana Shield in Suriname. *Geol. Mijnbouw* **62**, pp. 241–254.

Buchan, K.L., Halls, H.C. and Mortensen, K.J., 1996. Paleomagnetism, U/Pb geochronology, and geochemistry of Marathon dykes, superior Province, and comparison with the Fort Frances swarm. *Can. J. Earth. Sci.* **33**, pp. 1583–1595.

Briden, J.C., McClelland, E. and Rex, D.C., 1993. Proving the age of a paleomagnetic pole: the case of the Ntanga Ring structure, Malawi. *J. Geophys. Res.* **98**, pp. 1743–1749.

Chauvet, A., Guerrot, C., Alves da Silva, F. and Faure, M., 1997. 207Pb/206Pb and 40Ar/39Ar geochronology of the paleoproterozoic granites of the Rio Itapicuru greenstone Belt (Bahia, Brazil). *C. R. Acad. Sci. Paris* **324**, pp. 293–300.

Choubert, B., 1974. Le Precambrien des Guyanes. Mem. B.R.G.M. 81, 213 pp.

Constanzo-Alvarez, V. and Dunlop, D.J., 1988. Paleomagnetic evidence for post-2.55 Ga tectonic tilting and 1.1 Ga reactivation in the southern Kapuskasing zone, Ontario, Canada. *J. Geophys. Res.* **93** B8, pp. 9126–9136.

Dahl, P.S., 1996. The effects of composition on retentivity of argon and oxygen in hornblende and related amphiboles: a field-tested empirical model. *Geochim. Cosmochim. Acta* **60**, pp. 3687–3700.

Dahl, P.S., 1997. A crystal–chemical basis for Pb retention and fission-track annealing systematics in U-bearing minerals, with implications for geochronology. *Earth Planet. Sci. Lett.* **150**, pp. 277–290.

Dahlberg, E.H., 1987. Copper and phosphate mineralization in the Lower Proterozoic mobile belt of Backuis mountains, Upper Nickerie, western Suriname. *Geol. Mijnbouw* **66**, pp. 151–164.

Deckart, K., Féraud, G. and Bertrand, H., 1997. Age of Jurassic continental tholeiites of French Guyana, Surinam and Guinea: implications for the initial opening of the Central Atlantic Ocean. *Earth Planet. Sci. Lett.* **150**, pp. 205–220.

Egal, E., Milési, J.P., Vanderhaeghe, O., Ledru, P., Cocherie, A., Thiéblemont D., Cautru, J.P., Vernhet, Y., Hottin, A.M., Tegyey, M., Martel-Jantin, B., 1995. Ressources minérales et évolution lithostrucurale de la Guyane. Carte thématique minière au 1/100,000. Feuille Régina. Rapport B.R.G.M. R 38458, 66 pp.

Fedotova, M.A., Khramov, A.N., Pisakin, B.N. and Priyatkin, A.A., 1999. Early Proterozoic palaeomagnetism: new results from the intrusives and related rocks of the Karelian, Blomorian and Kola provinces, eastern Fennoscandian shield. *Geophys. J. Int.* **137**, pp. 691–712.

Féraud, G., Gastaud, J., Auzende, J.M., Olivet, J.L. and Comen, G., 1982. $^{40}Ar/^{39}Ar$ ages for the alkaline volcanism and the basement of Gorringe Bank, North Atlantic Ocean. *Earth Planet. Sci. Lett.* **57**, pp. 211–226.

Féraud, G., York, D., Mevel, C., Cornen, G., Hall, C.M. and Auzende, J.M., 1986. Additional $^{40}Ar/^{39}Ar$ dating of the basement and the alkaline volcanism of Gorringe bank (Atlantic Ocean). *Earth Planet. Sci. Lett.* **79**, pp. 255–269.

Fisher, R., 1953. Dispersion on a sphere. *Proc. R. Soc. Ser. A* **217**, pp. 295–305. MathSciNet

Gibbs, A.K., Baron C.N., 1993. The Geology of the Guiana Shield. Oxford Mono. Geol. Geophys. 22, 258 pp.

GPMDB, 1998. Global paleomagnetic database Access version (GPMDB version 3.3), Access versions of the GPMDB are given by McElhinny and Lock (1996).

Grove, M. and Harrison, T.M., 1996. $^{40}Ar^*$ diffusion in Fe-rich biotite. *Am. Mineral.* **81**, pp. 940–951.

Gruau, G., Martin, H., Leveque, B. and Capdevilla, R., 1985. Rb–Sr and Sm–Nd geochronology of lower Proterozoic granite–greenstone terrains in French Guiana. *Precambrian. Res.* **30**, pp. 63–80.

Harrison, T.M., 1981. Diffusion of ^{40}Ar in hornblende. *Contrib. Mineral. Petrol.* **78**, pp. 324–331.

Harrison, T.M., Duncan, I. and Mc Dougall, H., 1985. Diffusion of ^{40}Ar in biotite: temperature, pressure and compositional effects. *Geochim. Cosmochim. Acta* **49**, pp. 2461–2468.

Lee, J.K.W., Willians, I.S. and Ellis, D.J., 1997. Pb, U and Th diffusion in natural zircon. *Nature* **390**, pp. 159–161.

Kirschvink, J.L., 1981. The least-squares lines and plane and the analysis of paleomagnetic data. *Geophys. J. R. Astron. Soc.* **62**, pp. 699–718.

Kroonenberg, S.B., 1976. Amphibolite-facies and granulite-facies metamorphism in the Coeroeni Group, SW Suriname. *Geol. Mijnbouwkd. Dienst Suriname Meded.* **25**, pp. 109–289.

Ledru, P., Lasserre, J.L., Manier, E. and Mercier, D., 1991. The Lower Proterozoic of northern Guiana: revision of the lithology, transurrent tectonics and sedimentary basin dynamics. *Bull. Soc. Géol. France* **162**, pp. 627–636.

Marot, A. 1988. Carte géologique de la Guyane au 1/500 000.

Mertanen, S., Halls, H.C., Vuollo, J.I, Pesonen, L.J. and Stepanov, V.S., 1999. Paleomagnetism of 2.44 Ga mafic dykes in Russian Karelia, eastern Fennoscandian Shield — implications for continental reconstructions. *Precambrian Res.* **98**, pp. 197–221.

McElhinny, M.W. and Lock, J., 1996. IAGA paleomagnetic databases with Access. *Surv. Geophys.* **17**, pp. 757–791.

Milési, J.P., Egal, E., Ledru, P., Vernhet, Y., Thiéblemont, D., Cocherie, A., Tegyey, M., Martel-Santin, B. and Lagny, P., 1995. Les minéralisations du Nord de la Guyane Française dans leur cadre géologique. *Chron. Rech. Minière* **518**, pp. 5–58.

Min, K., Mundil, R., Renne, P.R. and Ludwig, K.R., 2000. A test for systematic errors in ^{40}Ar/^{39}Ar geochronology through comparison with U/Pb analysis of a 1.1 Ga rhyolite. *Geochim. Cosmochim. Acta* **64**, pp. 73–98.

Montgomery, C. and Hurley, P.M., 1978. Total rock U–Pb and Rb–Sr systematics in the Imataca Series. Guyana Shield, Venezuela. *Earth Planet. Sci. Lett.* **39**, pp. 281–290.

Nomade, S., Théveniaut, H., Chen, Y., Pouclet, A. and Rigollet, C., 2000. Paleomagnetic study of French Guyana Early Jurassic dolerites: hypothesis of a multistage magmatic event. *Earth Planet. Sci. Lett.* **184**, pp. 155–168.

Onstott, T.C. and Hargraves, R.B., 1981. Proterozoic transcurrent tectonics: palaeomagnetic evidence from Venezuela and Africa. *Nature* **289**, pp. 131–137.

Onstott, T.C., Hargraves, R.B., York, D. and Hall, C., 1984. Constraints on the notions of South America and African Shields during the Proterozoic: $^{40}Ar/^{39}Ar$ and paleomagnetic correlations between Venezuela and Liberia. *Geol. Soc. Am. Bull.* **95**, pp. 1045–1054.

Onstott, T.C., Hall, C.M. and York, D., 1989. $^{40}Ar/^{39}Ar$ thermochronology of the Imataca complex, Venezuela. *Precambrian Res.* **42**, pp. 255–291.

Raposo, M.I.B. and D'Agrella-Filho, M.S., 2000. Magnetic fabrics of dike swarms from SE Bahia State, Brazil: their significance and implications for mesoproterozoic basic magmatism in the São-Fransisco Craton. *Precambrian Res.* **99**, pp. 309–325.

Renne, P.R., 2000. $^{40}Ar/^{39}Ar$ age of plagioclase from Acapulco meteorite and the problem of systematic errors in cosmochronology. *Earth Planet. Sci. Lett.* **175**, pp. 13–26.

Ruffet, G., Féraud, G. and Amouric, M., 1991. Comparison of $^{40}Ar/^{39}Ar$ conventional and laser dating of biotites from the North Trégor Batholith. *Geochim. Cosmochim. Acta* **55**, pp. 1675–1688.

Steiger, R.H. and Jäger, E., 1977. Subcommission on geochronology: convention of the use of decay constants in geo- and cosmochronology. *Earth Planet. Sci. Lett.* **36**, pp. 359–362.

Swapp, S.M. and Onstott, T.C., 1989. *P–T*–Time characterization of the Trans-amazonian Orogeny in the Imataca Complex, Venezuela. *Precambrian Res.* **42**, pp. 293–314.

Teixieira, W., Tassiniari, C.C.G., Cordani, U.G. and Kawashita, K., 1989. A review of the geochronology of the Amazonian Craton: tectonic implications. *Precambrian Res.* **42**, pp. 213–227.

Torsvik, T.H. and Meert, J.G., 1995. Early Proterozoic palaeomagnetic data from the Pechenga Zone (north-west Russia) and their bearing on Early Proterozoic palaeogeography. *Geophys. J. Int.* **122**, pp. 520–536.

Turner, G., Huneke, J.C., Podosek, F.A. and Wasserburg, G.J., 1971. *40*Ar/*39*Ar ages and cosmic ray exposure ages of Apollo 14 samples. *Earth Planet. Sci. Lett.* **12**, pp. 19–35.

Vanderhaeghe, O., Ledru, P., Thiéblemont, D., Egal, E., Cocherie, A., Tegyey, M. and Milési, J.P., 1998. Contrasting mechanism of crustal growth, geodynamic evolution of the Paleoproterozoic granite-greenstone belts of French Guiana. *Precambrian Res.* **92**, pp. 165–193.

Zijderveld, J.D.A., 1967. Demagnetization of rock: analysis of results. In: Collinson, D.W., Creer, K.M. and Runcorn, S.K., Editors, 1967. *Methods in Paleomagnetism*, Elsevier, Amsterdam, pp. 254–286.